

End-Effector Stabilization of a 10-DOF Mobile Manipulator using Nonlinear Model Predictive Control

Mostafa Osman* Mohamed W. Mehrez* Shiyi Yang*
Soo Jeon* William Melek*

* Mechanical and Mechatronics Engineering, University of Waterloo,
Waterloo, Ontario, N2L 3G1, Canada (email: {meaosman,
mohamed.said, s268yang, soojeon, william.melek}@uwaterloo.ca)

Abstract: Motion control of mobile manipulators (a robotic arm mounted on a mobile base) can be challenging for complex tasks such as material and package handling. In this paper, a task-space stabilization controller based on Nonlinear Model Predictive Control (NMPC) is designed and implemented to a 10 Degrees of Freedom (DOF) mobile manipulator which consists of a 7-DOF robotic arm and a 3-DOF mobile base. The system model is based on kinematic models where the end-effector orientation is parameterized directly by a rotation matrix. The state and control constraints as well as singularity constraints are explicitly included in the NMPC formulation. The controller is tested using real-time simulations, which demonstrate high positioning accuracy with tractable computational cost.

Keywords: Mobile manipulator, task-space control, non-linear model predictive control

1. INTRODUCTION

The use of mobile manipulators in industry has increased drastically over the past decade. Mobile manipulators combine the advantages of both wheeled robots and robotic arms; thus, they have an expandable workspace and operational versatility through perception, object manipulation, and mobility. Such robots can be used in material handling, wall painting, as well as inspection and repairs, see, e.g. (Bostelman et al., 2016) for a survey. Operating such systems requires safe navigation in possibly dynamic environments and precise object manipulation. In this paper, we focus on stabilizing the end-effector of a 10-DOF mobile manipulator shown in Fig. 1. The mobile manipulator is built by integrating the Summit-XLS mobile robot with meccanum wheels manufactured by Robotnik and the 7-DOF Barrett WAM robotic arm.

The separate control of mobile robots and robotic arms is studied extensively in the literature. The considered control problems can be categorized under point-stabilization, trajectory tracking, and path following. The commonly used control techniques include feedback linearization (d'Andréa Novel et al., 1995), robust control (Koubaa et al., 2013), fuzzy based feedback linearization (Piltan et al., 2013), adaptive control (Pourboghrat and Karlsson, 2002; Slotine and Weiping, 1988), and model predictive control (MPC) (Faulwasser et al., 2016; Mehrez et al., 2020).

Several studies that consider controlling mobile manipulators as a combined system also exist. For example, Silva and Adorno (2016) designed a whole-body controller based on feedback linearization controlling the end-effector pose of a mobile manipulator. The controller was tested on a 7-

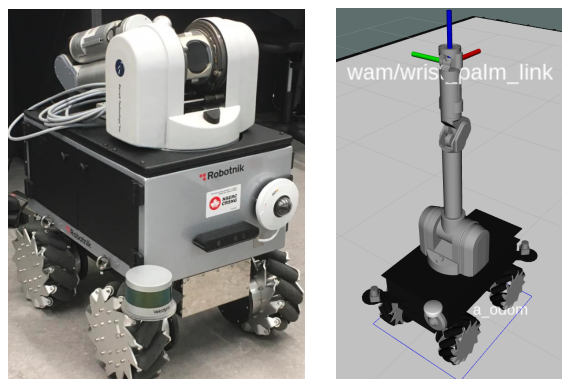


Fig. 1. The synthesized mobile manipulator. Left: the real robot. Right: the simulated robot.

DOF mobile manipulator. Patel et al. (2017) proposed an adaptive backstepping control for the trajectory tracking of mobile manipulators. Mishra et al. (2018) developed a robust nonlinear controller with uncertainty estimator; the controller was validated through simulations for a 7-DOF mobile manipulator. Furthermore, Avanzini et al. (2016) used linear MPC for developing a reactive constrained controller of an omnidirectional mobile base with a 5-DOF robotic arm. All the aforementioned studies considered mobile manipulators with non-redundant arms. This simplifies the problem due to the presence of a closed-form inverse kinematics solutions for such arms. Thus, the control of the mobile manipulator end-effector can be designed in the configuration (joint) space by utilizing a separate closed-form inverse kinematics module, see, e.g. (Avanzini et al., 2016).

MPC is popular in the field of controls because of its ability to handle constrained possibly nonlinear multi-input-multi-output (MIMO) systems. In MPC, a cost function characterizing the control objective is minimized using an open-loop control sequence or function while state and control constraints are considered. The first part of the resulting open-loop control is then applied to the system. Finally, the process is repeated every decision instant, see, e.g. (Allgöwer and Zheng, 2012).

In this paper, we use a nonlinear model predictive control (NMPC) scheme to stabilize the end-effector of a 10-DOF mobile manipulator; here, we first formulate the task-space kinematic model, where the overall system rotations are expressed using the 3D special orthogonal $SO(3)$ representation. Then, this model is used for state prediction in the NMPC formulation, which considers state and control constraints as well as kinematic singularity constraints. The proposed NMPC controller is implemented using Robot Operating System (ROS) (Quigley et al., 2009) and the efficacy of the proposed controller is demonstrated through a series of real-time simulations using Gazebo dynamic simulator (Koenig and Howard, 2004). The results show highly-accurate and smooth stabilization of the end-effector as well as computational cost, which meets the real-time requirements.

The remainder of the paper is organized as follows: the model used to implement the NMPC is explained in Section 2 followed by the optimal control (OCP) problem formulation in Section 3. In Section 4, the simulation testbed used to validate the proposed controller is introduced and then the acquired results are shown in Section 5. Finally, in Section 6 conclusions are stated and the future work is summarized.

2. MOBILE MANIPULATOR MODELING

In this section, we, first, show the notations used in the paper. Then, we present the kinematic model of the synthesized mobile manipulator.

2.1 Notations

\mathbb{N} and \mathbb{R} denote the sets of natural and real numbers, respectively, $\|x\|_\infty$ is the l_∞ norm defined as $\|x\|_\infty := \max_{i \in [1:n]} |x_i|$, $\|x\|_A^2$ is the squared l_2 norm weighted by A and is calculated as $x^\top A x$, the matrix trace operator is denoted by Tr , $A \succ 0$ denotes that A is a positive definite matrix, $\mathbf{I}_{n \times n}$ is the $n \times n$ identity matrix, $\mathbf{0}_{n \times k}$ denotes an $n \times k$ matrix with all entries of zeros, and $SO(3)$ and $SE(3)$ denote the special orthogonal and special Euclidean groups, respectively.

2.2 Kinematic Model of the holonomic Mobile Base

The mobile base of the considered mobile manipulator is a holonomic mobile robot with meccanum wheels. Holonomic mobile robots possess an extra degree of maneuverability when compared to the non-holonomic robots (Siegwart et al., 2011).

The discrete-time kinematic model of the mobile base is given by

$$\begin{aligned} \mathbf{x}_{k+1}^b &= \mathbf{f}_{mr}(\mathbf{x}_k^b, \mathbf{u}_k) \\ &= \begin{bmatrix} x_k^b \\ y_k^b \\ \gamma_k \end{bmatrix} + \tau \underbrace{\begin{bmatrix} \cos \gamma_k & -\sin \gamma_k & 0 \\ \sin \gamma_k & \cos \gamma_k & 0 \\ 0 & 0 & 1 \end{bmatrix}}_{R_b^I} \begin{bmatrix} u_{1,k} \\ u_{2,k} \\ u_{3,k} \end{bmatrix}, \end{aligned} \quad (1)$$

where $\mathbf{x}^b = (x, y, \gamma)^\top \in X_{mr} \subset \mathbb{R}^3$ is the pose of the mobile base in the inertial frame, (x^b, y^b) are the two Cartesian planar coordinates and γ is the yaw angle of the mobile base. $\mathbf{u} = (u_1, u_2, u_3)^\top \in U_{mr} \subset \mathbb{R}^3$ is the robot input speeds, $\mathbf{f}_{mr} : \mathbb{R}^3 \times \mathbb{R}^3 \rightarrow \mathbb{R}^3$ is a nonlinear mapping, $R_b^I \in SO(3)$ is the z -axis rotation matrix, and $\tau > 0$ is the sampling time.

The state constraint set X_{mr} is a compact set defined as

$$X_{mr} := [\underline{x}^b, \bar{x}^b] \times [\underline{y}^b, \bar{y}^b] \times [-\pi, \pi],$$

where $\underline{x}^b, \bar{x}^b, \underline{y}^b, \bar{y}^b$ are the lower and upper bounds of the Cartesian coordinates x^b and y^b , respectively.

The relation between the robot input speeds \mathbf{u} and wheel speeds $\mathcal{V} = (\omega_1, \omega_2, \omega_3, \omega_4)^\top$, for meccanum wheels robots, can be stated as (Lynch and Park, 2017)

$$\mathcal{V} := \begin{bmatrix} \omega_1 \\ \omega_2 \\ \omega_3 \\ \omega_4 \end{bmatrix} = H \mathbf{u} = \frac{1}{r} \begin{bmatrix} 1 & -1 & -l - w \\ 1 & 1 & l + w \\ 1 & -1 & l + w \\ 1 & 1 & -l - w \end{bmatrix} \mathbf{u}, \quad (2)$$

where r is the meccanum wheel radius, l and w are half of the wheelbase and the trackwidth, respectively. Consequently, the control constraint set U_{mr} is a compact set defined as

$$U_{mr} := \{\mathbf{u} \in \mathbb{R}^3 \mid \|H \mathbf{u}\|_\infty \leq \omega_{max}\}, \quad (3)$$

where ω_{max} is the rated speed of the wheel motors.

2.3 Kinematic Model of the Robotic Arm

The robotic arm mounted on the aforementioned mobile base is a 7-DOF WAM arm by Barrett Technology (Barrett, 2018a). The end-effector pose of the robotic arm is denoted by $\mathbf{x}^a := [\mathbf{p}^{a\top}, \theta^{a\top}]^\top$, where $\mathbf{p}^a \in \mathbb{R}^3$ is the end-effector position in the robotic arm base frame represented in the Cartesian coordinates and θ^a is the end-effector orientation. The end-effector orientation can be represented using several methods as discussed in (Campa and De La Torre, 2009). Here, we use the $SO(3)$ group to avoid representation singularities and error definition discontinuities. To do so, we define the mapping function $f : SO(3) \rightarrow \mathcal{F} \subset \mathbb{R}^9$, such that, for a rotation matrix $R \in SO(3)$,

$$f(R) = [[R]_1^\top \ [R]_2^\top \ [R]_3^\top]^\top, \quad (4)$$

where $[R]_i$, $i \in \{1, 2, 3\}$, is the i -th column vector of the rotation matrix R . Thus, the orientation vector θ^a is $\theta^a = f(R_E^b) \in \mathcal{F}$, and R_E^b is the rotation matrix of the end-effector in the base frame of the robotic arm.

Using such a representation, the kinematic model of the robotic arm can be described using the analytical Jacobian \mathbf{J}_a of the forward kinematics transformation matrix $\mathbf{T} \in SE(3)$ derived using the DH-parameters of the robotic arm, (see Barrett (2018b) for the DH-parameters of the considered robotic arm), as

$$\mathbf{x}_{k+1}^a = \mathbf{f}_{ra}(\mathbf{x}_k^a, \mathbf{q}_k, \dot{\mathbf{q}}_k) = \mathbf{x}_k^a + \tau \mathbf{J}_a(\mathbf{q}_k) \dot{\mathbf{q}}_k, \quad (5)$$

where $\mathbf{x}^a = [\mathbf{p}^{a\top}, \theta^{a\top}]^\top \in X_{ra} \subset \mathbb{R}^{12}$ is the state vector defined using θ^a from (4), $\mathbf{q} = [q_1, q_2, q_3, q_4, q_5, q_6, q_7]^\top \in Q \subset \mathbb{R}^7$ is the joint angles vector, $\dot{\mathbf{q}} \in \Omega \subset \mathbb{R}^7$ is the joint velocities vector, and, the analytical Jacobian \mathbf{J}_a is given by $\mathbf{J}_a := \partial \mathbf{T} / \partial \mathbf{q}$.

The constraint sets for the end-effector X_{ra} , joint angles Q , and joint velocities Ω are defined by

$$\begin{aligned} X_{ra} &:= [\underline{x}^a, \bar{x}^a] \times [\underline{y}^a, \bar{y}^a] \times [\underline{z}^a, \bar{z}^a] \times \mathcal{F}, \\ Q &:= \{\mathbf{q} \in \mathbb{R}^7 \mid q_i \leq \bar{q}_i, \forall i \in \{1, \dots, 7\}\}, \\ \Omega &:= \{\dot{\mathbf{q}} \in \mathbb{R}^7 \mid \|\dot{\mathbf{q}}\|_\infty \leq \dot{q}_{max}\}, \end{aligned}$$

where \underline{q}_i and \bar{q}_i denote the lower and upper limits of the joint angles, respectively.

In order to be able to keep track of the joint angles and consider joint constraints, we extend system (5) to

$$\begin{bmatrix} \mathbf{x}_{k+1}^a \\ \mathbf{q}_{k+1} \end{bmatrix} = \begin{bmatrix} \mathbf{x}_k^a \\ \mathbf{q}_k \end{bmatrix} + \tau \begin{bmatrix} \mathbf{J}_a(\mathbf{q}) \\ \mathbf{I}_{7 \times 7} \end{bmatrix} \dot{\mathbf{q}}_k, \quad (6)$$

where $[\mathbf{x}^{a\top}, \mathbf{q}^\top]^\top \in \bar{X}_{ra} \subset \mathbb{R}^{19}$ is the concatenated state vector, and \bar{X}_{ra} is the state constraint set for the new augmented model and is defined as $\bar{X}_{ra} := X_{ra} \times Q$.

2.4 Mobile Manipulator Kinematic Model

The model of the mobile manipulator can now be derived using the model of the mobile base and the robotic arm. First, we map the velocity components of the mobile base to the end-effector linear speeds in the inertial frame, i.e. we have

$$\dot{\mathbf{p}}^b = [R_b^I]_{2 \times 2} \begin{bmatrix} u_1 \\ u_2 \end{bmatrix} + \underbrace{[R_b^I]_{2 \times 2}}_{\psi} \begin{bmatrix} -y_E^b \\ x_E^b \end{bmatrix} u_3 \quad (7)$$

where $\dot{\mathbf{p}}^b = [\dot{x}^b, \dot{y}^b]$ is the linear velocity of the end-effector caused by the mobile base in the inertial frame, and $[R_b^I]_{2 \times 2}$ is the upper left 2×2 sub-matrix of R_b^I shown in Eq. (1). Note that R_b^I is the orientation of the mobile robot, which can be determined through the localization feedback. x_E^b, y_E^b are the position of the end-effector in the mobile base frame and can be determined from the forward kinematics transformation matrix \mathbf{T} .

Second, to calculate the angular velocity of the mobile robot in $SO(3)$, we need to calculate the derivative of the rotation matrix R_b^I . As mentioned in (Campa and De La Torre, 2009), the derivative of a rotation matrix R can be calculated as

$$\dot{R} = S(\omega)R, \quad (8)$$

where $S(\omega)$ is the skew symmetric matrix form of the angular velocity vector $\omega = [\omega_x, \omega_y, \omega_z]^\top$, where ω_x, ω_y and ω_z are the three angular velocities around the principle axes x, y and z , respectively. Using the properties of the skew-symmetric matrix, Eq. (8) can be written as

$$\dot{\theta}^b := \begin{bmatrix} \dot{R}_1 \\ \dot{R}_2 \\ \dot{R}_3 \end{bmatrix} = - \underbrace{\begin{bmatrix} S([R]_1) \\ S([R]_2) \\ S([R]_3) \end{bmatrix}}_{=: \Theta \in \mathbb{R}^{9 \times 3}} \omega, \quad (9)$$

where $\dot{\theta}^b$ is the rate of change of the end-effector orientation due to the mobile base rotation. Moreover, $S([R]_n)$ is the n -th column vector of R in the skew symmetric form.

Since we do not consider any other angular velocities than w_z for the mobile base, the first two columns of Θ in (9) will be zeros. Consequently, $\dot{\theta}^b$ reads

$$\dot{\theta}^b := \begin{bmatrix} \dot{R}_b^I \\ \dot{R}_b^I \\ \dot{R}_b^I \end{bmatrix}_3 = - \underbrace{\begin{bmatrix} S([R_b^I]_1) \\ S([R_b^I]_2) \\ S([R_b^I]_3) \end{bmatrix}}_{=: \Theta_3 \in \mathbb{R}^{9 \times 1}} u_3, \quad (10)$$

where we exploit the fact that w_z for an omnidirectional mobile robot is the control action u_3 shown in Eq. (1).

Using Eq. (7) and (10), in addition to the kinematic model in Eq. (6), the kinematic model of the whole mobile manipulator can be written as

$$\begin{aligned} \begin{bmatrix} \mathbf{x}_{k+1} \\ \mathbf{q}_{k+1} \end{bmatrix} &= \begin{bmatrix} \mathbf{x}_k \\ \mathbf{q}_k \end{bmatrix} + \tau \mathbf{J}_{mm}(\mathbf{x}_k, \mathbf{q}_k) \begin{bmatrix} \mathbf{u}_k \\ \dot{\mathbf{q}}_k \end{bmatrix} \\ &= \underbrace{\begin{bmatrix} \mathbf{x}_k \\ \mathbf{q}_k \end{bmatrix} + \tau \begin{bmatrix} [R_b^I]_{2 \times 2} & \psi & \mathbf{J}_a(\mathbf{q}_k) \\ \mathbf{0}_{10 \times 2} & -\Theta_3 & \mathbf{I}_{7 \times 7} \end{bmatrix}}_{\mathbf{f}_{mm}(\mathbf{x}_k, \mathbf{q}_k, \mathbf{u}_k, \dot{\mathbf{q}}_k)} \begin{bmatrix} \mathbf{u}_k \\ \dot{\mathbf{q}}_k \end{bmatrix}, \end{aligned} \quad (11)$$

where $[\mathbf{x}^\top, \mathbf{q}^\top]^\top \in X \subset \mathbb{R}^{19}$ is the concatenated state vector of the mobile manipulator, $[\mathbf{u}, \dot{\mathbf{q}}^\top]^\top \in U \subset \mathbb{R}^{10}$ is the concatenated control vector. Here, $\mathbf{x} := [\mathbf{p}^\top, \theta^\top]^\top$ is the end-effector pose vector in the inertial frame.

The model stated in (11) is the complete kinematic model of the considered 10-DOF mobile manipulator consisting of a 3-DOF holonomic mobile base and a 7-DOF robotic arm. The constraints over the developed kinematic model can now be defined as

$$\begin{aligned} X &:= [x, \bar{x}] \times [y, \bar{y}] \times [z, \bar{z}] \times \mathcal{F} \times Q, \text{ and} \\ U &:= U_{mr} \times \Omega. \end{aligned} \quad (12)$$

Finally, the end-effector pose feedback can be determined by the pose of the mobile robot determined through the use of a localization algorithm (Osman et al., 2019) and the forward kinematic equations of the robotic arm \mathbf{T} .

3. NONLINEAR MODEL PREDICTIVE CONTROL

In this section, we formulate an NMPC scheme for the end-effector pose stabilization of the mobile manipulator. To this end, we define

$$\begin{aligned} \mathcal{U}_N &:= \left(\begin{bmatrix} \mathbf{u}_k \\ \dot{\mathbf{q}}_k \end{bmatrix}, \begin{bmatrix} \mathbf{u}_{k+1} \\ \dot{\mathbf{q}}_{k+1} \end{bmatrix}, \dots, \begin{bmatrix} \mathbf{u}_{k+N-1} \\ \dot{\mathbf{q}}_{k+N-1} \end{bmatrix} \right) \text{ and} \\ \mathcal{X}_N &:= (\mathbf{x}_k, \mathbf{x}_{k+1}, \dots, \mathbf{x}_{k+N}) \end{aligned}$$

as the sequences of controls and states over the prediction horizon $N \in \mathbb{N}$, respectively. As standard in NMPC, these sequences are used to form the quadratic cost function

$$\begin{aligned} J(\mathcal{U}_N, \mathcal{X}_N) &= \underbrace{\|\mathcal{E}_N^{\mathbf{p}}\|_{\mathcal{S}^{\mathbf{p}}}^2 + \|\mathcal{E}_N^{\theta}\|_{\mathcal{S}^{\theta}}^2}_{J_f} \\ &+ \sum_{i=k}^{k+N-1} \|\mathcal{E}_k^{\mathbf{p}}\|_{\mathcal{Q}^{\mathbf{p}}}^2 + \|\mathcal{E}_k^{\theta}\|_{\mathcal{Q}^{\theta}}^2 + \left\| \begin{bmatrix} \mathbf{u}_i \\ \dot{\mathbf{q}}_i \end{bmatrix} \right\|_{\mathcal{R}}^2, \end{aligned} \quad (13)$$

where $\mathcal{S}^{\mathbf{p}} \in \mathbb{R}^{3 \times 3} \succ 0$, $\mathcal{S}^{\theta} \in \mathbb{R}^{9 \times 9} \succ 0$, $\mathcal{Q}^{\mathbf{p}} \in \mathbb{R}^{3 \times 3} \succ 0$, $\mathcal{Q}^{\theta} \in \mathbb{R}^{9 \times 9} \succ 0$ and $\mathcal{R} \in \mathbb{R}^{10 \times 10} \succ 0$ are the weighting matrices of the quadratic cost function, and J_f is the terminal cost of the cost function. $\mathcal{E}^{\mathbf{p}} \in \mathbb{R}^3$ is

the translational error of the end-effector pose defined as $\mathcal{E}^p := \mathbf{p} - \mathbf{p}^r$, where \mathbf{p}^r is the reference position, and $\mathcal{E}^\theta \in \mathbb{R}^9$ is the orientation error of the end-effector pose defined as

$$\mathcal{E}^\theta := \begin{bmatrix} [I_{3 \times 3}]_1 \\ [I_{3 \times 3}]_2 \\ [I_{3 \times 3}]_3 \end{bmatrix} - \begin{bmatrix} [(R_E^I)^\top R_r]_1 \\ [(R_E^I)^\top R_r]_2 \\ [(R_E^I)^\top R_r]_3 \end{bmatrix}, \quad (14)$$

where R_r is the reference orientation, and R_E^I is the orientation of the end-effector in the inertial frame calculated as $R_E^I = R_b^I R_E^b$. R_b^I is determined using a localization algorithm of the mobile robot and R_E^b is the rotation matrix from the mobile robot to the end-effector and is calculated from the forward kinematics of the robotic arm, i.e. \mathbf{T} .

Using the cost function in Eq. (13), the NMPC optimal control problem can be formulated as:

$$(\mathcal{U}_N^*, \mathcal{X}_N^*) = \arg \min_{\mathcal{U}_N \in U, \mathcal{X}_N \in X} J(\mathcal{U}_N, \mathcal{X}_N) \quad (15a)$$

$$\text{subject to } [\mathbf{x}_{k+1} \ \mathbf{q}_{k+1}]^\top - \mathbf{f}_{mm}(\mathbf{x}_k, \mathbf{q}_k, \mathbf{u}_k, \dot{\mathbf{q}}_k) = 0, \quad (15b)$$

$$\mathcal{X}_N \in X \subseteq \mathbb{R}^{19}, \quad (15c)$$

$$\mathcal{U}_N \in U \subseteq \mathbb{R}^{10}, \quad (15d)$$

$$|\det(\mathbf{J}_a \mathbf{J}_a^\top)| > \epsilon \quad (15e)$$

where ϵ is a threshold for avoiding singular configurations of the robotic arm.

OCP (15) is converted to a nonlinear programming problem (NLP) using the direct multiple-shooting method (Albersmeyer and Diehl, 2010). Here, both the control sequence \mathcal{U}_N as well as the state sequence \mathcal{X}_N are considered as decision variables in the optimization problem. Moreover, the system model is considered as an optimization constraint as formulated by Eq. (15b). Multiple-shooting discretization technique provides a more computationally efficient solution to OCP (15) when compared with other discretization techniques, e.g. single-shooting, see (Albersmeyer and Diehl, 2010) for more details. Finally, state and control constraints are considered by means of Eq. (15c) and (15d). Note that the inequality constraint (15e) is added to avoid kinematic singularities of the robotic arm through operation. This is accomplished through ensuring that the pseudo-inverse of the robot arm Jacobian matrix is always invertible and, thus, singular configurations are avoided.

The feedback control law can now be stated as

$$[\mathbf{u}_k^* \ \dot{\mathbf{q}}_k^*]^\top := \mathcal{U}_N^*(0),$$

i.e. the feedback control is the first element in the optimal control sequence \mathcal{U}_N^* . Moreover, the resulting feedback system can be stated as

$$[\mathbf{x}_{k+1} \ \mathbf{q}_{k+1}]^\top = \mathbf{f}_{mm}(\mathbf{x}_k, \mathbf{q}_k, \mathbf{u}_k^*, \dot{\mathbf{q}}_k^*).$$

4. REAL-TIME SIMULATION TESTBED AND SIMULATION SCENARIOS

The simulation testbed of the considered mobile manipulator is created by synthesizing the “urdf” models of both the Barret WAM arm and the Summit XLS mobile robot in a ROS/Gazebo simulation environment¹. Here,

¹ urdf: universal robotic description format.

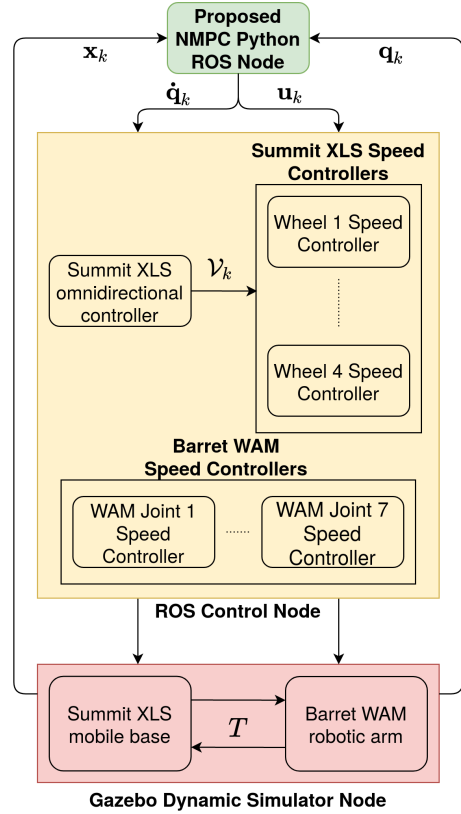


Fig. 2. Block-diagram of ROS/Gazebo dynamic simulation environment used to validate the proposed controller.

the transformation and the constraints between the two models are defined based on the actual physical system, see Fig. 1. Moreover, the proposed NMPC controller is programmed in python programming language and integrated with the simulation environment via a ROS-node. Here, OCP (15) is formulated symbolically using the numerical optimization software tool CasADi (Andersson et al., 2018). Additionally, OCP (15) is solved using the interior-point optimization method via the open source solver IPOPT (Wächter and Biegler, 2006). The overall block-diagram of the ROS/Gazebo real-time simulation environment is illustrated in Fig. 2.

The scenarios shown in Table 1 were used to validate the proposed controller. Initial and set-point references shown are presented using the Z-Y-X Euler angles to simplify the presentation. In all scenarios, the sampling time is $\tau = 0.15$ sec, the prediction horizon is $N = 5$, and the weighting matrices are $\mathcal{S}^p, \mathcal{Q}^p = 2\mathbf{I}_{3 \times 3}$, $\mathcal{S}^\theta, \mathcal{Q}^\theta = 15\mathbf{I}_{9 \times 9}$

Table 1. Real-time simulation scenarios

Scenario	Initial States	Reference Pose
1	$[2, 0, 1.42, 0, 0, 0]^\top$	$[0, 0, 0.5, \pi, 0, 0]^\top$
2	$[2, 2, 1.42, 0, 0, 0]^\top$	$[0, 0, 0.5, \pi/2, 0, 0]^\top$
3	$[0, 2, 1.42, 0, 0, 0]^\top$	$[0, 0, 0.5, 0, \pi/2, 0]^\top$
4	$[-2, 2, 1.42, 0, 0, 0]^\top$	$[0, 0, 0.5, 0, \pi, 0]^\top$
5	$[-2, 0, 1.42, 0, 0, 0]^\top$	$[0, 0, 0.5, 0, 0, \pi/2]^\top$
6	$[-2, -2, 1.42, 0, 0, 0]^\top$	$[0, 0, 0.5, 0, 0, \pi]^\top$
7	$[0, -2, 1.42, 0, 0, 0]^\top$	$[0, 0, 0.5, 0, 0, 0]^\top$
8	$[2, -2, 1.42, 0, 0, 0]^\top$	$[0, 0, 0.5, \pi, 0, 0]^\top$

and $\mathcal{R} = \mathbf{I}_{10 \times 10}$. Furthermore, the constraints set X defined in (12) is chosen as

$$X = [-3, 3] \times [-3, 3] \times [0.4, 1.43] \times \mathcal{F} \times Q,$$

where the arm joint angles limits set Q is given by

$$Q = \left\{ \begin{bmatrix} -2.6 \\ -1.985 \\ -2.8 \\ -0.9 \\ -4.55 \\ -1.5707 \\ -3.0 \end{bmatrix} \leq \mathbf{q} \leq \begin{bmatrix} 2.6 \\ 1.985 \\ 2.8 \\ \pi \\ 1.25 \\ \pi/2 \\ 3.0 \end{bmatrix} \right\}.$$

Here, the joint angle limits are adapted from the arm specifications (Barrett, 2018a). Finally, the limit of the joints speeds is chosen as $\dot{q}_{max} = 0.5$ rad/sec and the angular speed limit of the mobile robot wheels is chosen as $\omega_{max} = 0.6$ rad/sec.

5. RESULTS AND DISCUSSION

In this section, we show the closed-loop results of the mobile manipulator under the NMPC controller for all the scenarios stated in Table 1. Fig. 3 shows the trajectory of the end-effector through each simulation case. As shown in the figure, the controller successfully stabilized the end-effector of the mobile manipulator to the desired position. The performance of the NMPC controller is evaluated by both position and orientation errors of the end-effector with respect to the reference pose. The positional error is measured by the Euclidean distance between the end-effector position and the reference position, while the orientation error is measured by the evaluation metric

$$E^\theta = 3 - \text{Tr}(R_E^I R_r^T), \quad (16)$$

where the trace of the error rotation matrix is used. In essence, Eq. (16) indicates that the orientation error E^θ converges to zero as the end-effector orientation R_E^I converges to the reference orientation R_r .

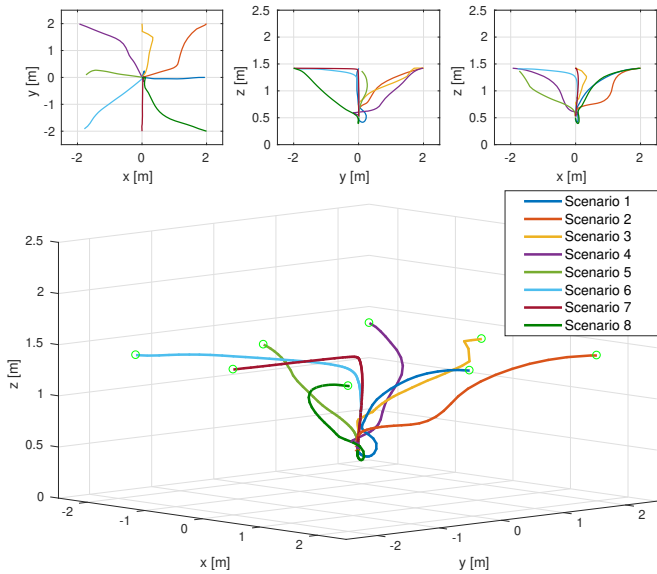


Fig. 3. The position trajectories of the end-effector for all the scenarios. Bottom: 3D visualization of the trajectories taken by the end-effector. Top: The three projected views of the end-effector trajectories.

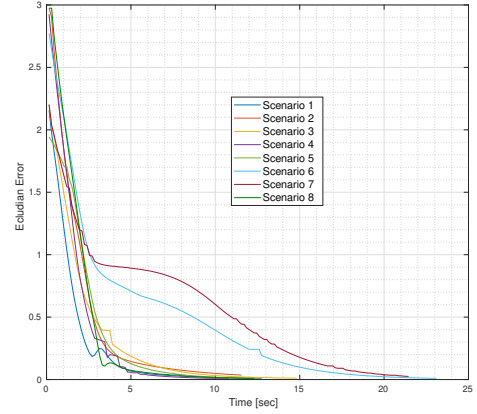


Fig. 4. Positional error (in meters) of the end-effector.

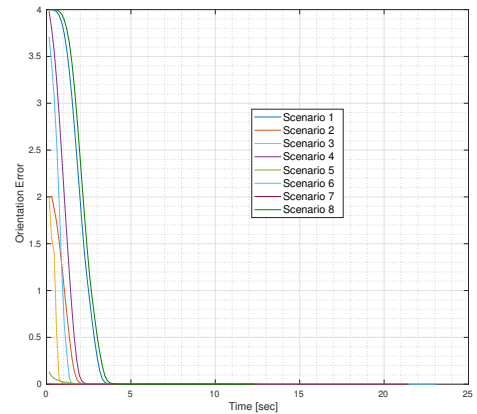


Fig. 5. Orientation error of the end-effector for all scenarios.

As shown in Fig. 4, the positional error converges to zero for all scenarios considered. Note that in scenarios 6 and 7, the settling time of the controller is relatively larger than that for the other scenarios due to the joints limits. In these two cases, the mobile manipulator had to take a longer maneuver to reach the required position and orientation without violating any joint limits. In Fig. 5, the orientation error of the end-effector, i.e. E^θ , is shown. The error is calculated using the evaluation metric stated in (16). As can be seen in the figure, the controller managed to quickly achieve all the required orientations.

All the real-time simulations were executed using an Intel Core i7 CPU with 2.10 GHz processor. The average computation time of OCP (15) throughout all the simulation scenarios was 61 ms with a maximum computation time of 130 ms and a standard deviation of 23.9 ms. Considering that the sampling time used is $\tau = 150$ ms, the computational results suggest that the proposed NMPC algorithm meets the real-time implementation requirements while generating feasible solutions.

6. CONCLUSION AND FUTURE WORK

In this paper, we proposed an NMPC controller for end-effector stabilization of a 10-DOF mobile manipulator. We used the kinematic models for both the mobile base and the robot arm to realize a task-space control for the end-effector of the mobile manipulator. Required constraints were directly considered, which include the joint limits and the manipulator singularity. We remark that using

the developed model along with NMPC, the stabilization of the end-effector was achieved without the need of any inverse kinematics solvers. Therefore, the proposed controller is a stand-alone high level controller, which only requires the localization feedback of the mobile base and the joint positions feedback of the robotic arm to operate on the mobile manipulator.

The controller was validated through real-time dynamic simulation scenarios. The results showed efficacy and efficiency of the proposed NMPC controller. Throughout all the designed scenarios, the controller managed to smoothly stabilize the end-effector to the required pose.

As for the future work, experiments using the real platform in Fig. 1 will be designed and performed to further validate the controller.

ACKNOWLEDGMENTS

We acknowledge the support of the Natural Sciences and Engineering Research Council of Canada (NSERC), [funding reference numbers PDF-532957-2019 (M.W. Mehrez), STPGP 506987 (S. Jeon)].

REFERENCES

- Albersmeyer, J. and Diehl, M. (2010). The lifted newton method and its application in optimization. *SIAM Journal on Optimization*, 20(3), 1655–1684.
- Allgöwer, F. and Zheng, A. (2012). *Nonlinear model predictive control*, volume 26. Birkhäuser.
- Andersson, J.A.E., Gillis, J., Horn, G., Rawlings, J.B., and Diehl, M. (2018). CasADi – A software framework for nonlinear optimization and optimal control. *Mathematical Programming Computation*.
- Avanzini, G.B., Zanchettin, A.M., and Rocco, P. (2016). Reactive constrained model predictive control for redundant mobile manipulators. In *Intelligent Autonomous Systems 13*, 1301–1314. Springer.
- Barrett (2018a). WAM Arm Specifications. URL <https://advanced.barrett.com/wam-arm-1>.
- Barrett (2018b). WAM Arm User Guide. URL http://www.me.unm.edu/~starr/research/WAM_UsersGuide_AE-00.pdf.
- Bostelman, R., Hong, T., and Marvel, J. (2016). Survey of research for performance measurement of mobile manipulators. *Journal of Research of the National Institute of Standards and Technology*, 121, 342–366.
- Campa, R. and De La Torre, H. (2009). Pose control of robot manipulators using different orientation representations: A comparative review. In *2009 American Control Conference*, 2855–2860. IEEE.
- d’Andréa Novel, B., Campion, G., and Bastin, G. (1995). Control of nonholonomic wheeled mobile robots by state feedback linearization. *The International journal of robotics research*, 14(6), 543–559.
- Faulwasser, T., Weber, T., Zometa, P., and Findeisen, R. (2016). Implementation of nonlinear model predictive path-following control for an industrial robot. *IEEE Transactions on Control Systems Technology*, 25(4), 1505–1511.
- Koenig, N. and Howard, A. (2004). Design and use paradigms for gazebo, an open-source multi-robot simulator. In *2004 IEEE/RSJ International Conference on Intelligent Robots and Systems (IROS)(IEEE Cat. No. 04CH37566)*, volume 3, 2149–2154. IEEE.
- Koubaa, Y., Boukattaya, M., and Damak, T. (2013). Robust control of wheeled mobile robot in presence of disturbances and uncertainties. In *14th International Conference on Sciences and Techniques of Automatic Control & Computer Engineering-STA’2013*, 274–280. IEEE.
- Lynch, K.M. and Park, F.C. (2017). *Modern Robotics: Mechanics, Planning, and Control*. Cambridge University Press, New York, NY, USA, 1st edition.
- Mehrez, M.W., Worthmann, K., Cenerini, J.P., Osman, M., Melek, W.W., and Jeon, S. (2020). Model predictive control without terminal constraints or costs for holonomic mobile robots. *Robotics and Autonomous Systems*, 127, 103468.
- Mishra, S., Londhe, P., Mohan, S., Vishvakarma, S., and Patre, B. (2018). Robust task-space motion control of a mobile manipulator using a nonlinear control with an uncertainty estimator. *Computers & Electrical Engineering*, 67, 729–740.
- Osman, M., Hussein, A., and Al-Kaff, A. (2019). Intelligent vehicles localization approaches between estimation and information: A review. In *2019 IEEE International Conference of Vehicular Electronics and Safety (ICVES)*, 1–8. IEEE.
- Patel, B., Pan, Y.J., and Ahmad, U. (2017). Adaptive backstepping control approach for the trajectory tracking of mobile manipulators. In *2017 IEEE International Conference on Robotics and Biomimetics (RO-BIO)*, 1769–1774. IEEE.
- Piltan, F., Yarmahmoudi, M., Mirzaie, M., Emamzadeh, S., and Hivand, Z. (2013). Design novel fuzzy robust feedback linearization control with application to robot manipulator. *International Journal of Intelligent Systems and Applications*, 5(5), 1.
- Pourboghraat, F. and Karlsson, M.P. (2002). Adaptive control of dynamic mobile robots with nonholonomic constraints. *Computers & Electrical Engineering*, 28(4), 241–253.
- Quigley, M., Gerkey, B., Conley, K., Faust, J., Foote, T., Leibs, J., Berger, E., Wheeler, R., and Ng, A. (2009). Ros: an open-source robot operating system. In *Proc. of the IEEE Intl. Conf. on Robotics and Automation (ICRA) Workshop on Open Source Robotics*. Kobe, Japan.
- Siegwart, R., Nourbakhsh, I.R., Scaramuzza, D., and Arkin, R.C. (2011). *Introduction to autonomous mobile robots*. MIT press.
- Silva, F.F.A. and Adorno, B.V. (2016). Whole-body control of a mobile manipulator using feedback linearization based on dual quaternions. In *2016 XIII Latin American Robotics Symposium and IV Brazilian Robotics Symposium (LARS/SBR)*, 293–298. IEEE.
- Slotine, J.J. and Weiping, L. (1988). Adaptive manipulator control: A case study. *IEEE transactions on automatic control*, 33(11), 995–1003.
- Wächter, A. and Biegler, L.T. (2006). On the implementation of an interior-point filter line-search algorithm for large-scale nonlinear programming. *Mathematical Programming*, 106(1), 25–57.